Cerium-doped zirconium dioxide, a visible-light-sensitive photoactive material of third generation

Cerium Doped Zirconium Dioxide, a Visible-Light Sensitive Photoactive Material of Third Generation

Chiara Gionco[1], Maria C. Paganini[1], Elio Giamel1o[1], Robertson Burgess[2], Cristiana Di Valentin[2], Gianfranco Pacchioni[2].*

[1] Dipartimento di Chimica, Università di Torino and NIS, Nanostructured Interfaces and Surfaces, Via P. Giuria 7, 10125 Torino, Italy

[2]Dipartimento di Scienza dei Materiali, Università di Milano-Bicocca, Via R. Cozzi, 53, 20125, Milano, Italy

If more than one address, use symbols to match author names to address(es).

AUTHOR INFORMATION

Corresponding Author

* elio.giamello@unito.it.

Present Addresses

†If an author's address is different than the one given in the affiliation line, this information may be included here.

ABSTRACT. The dispersion of small amounts of Ce^{4+} ions in the bulk of ZrO_2 leads to a photoactive material sensitive to visible light. This is shown monitoring by EPR the formation and the reactivity of photogenerated (λ>420nm) charge carriers. The effect is due to the presence of empty 4f Ce states at mid gap which act as intermediate levels in a two-photon excitation mechanism. This solid can be considered an example of third generation photoactive material.

TOC GRAPHICS

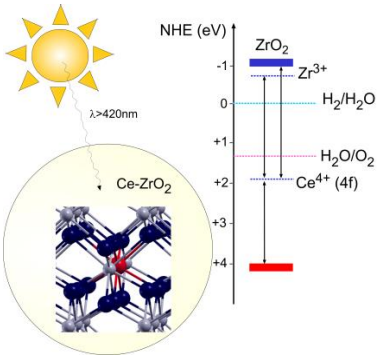

KEYWORDS Charge separation, DFT, EPR spectroscopy, Third generation photoactive systems.

Photocatalytic reactions have enormous importance in modern environmental chemistry (oxidative removal of pollutants of emergent concern)[1] and energetics[2]. In particular, the photo-electrochemical splitting of water achieved by Fujishima and Honda in 1972[3] using a TiO_2 photoanode paved the avenue to a new, stimulating research branch known as artificial photosynthesis[4]. Pristine TiO_2 is even now the dominant system in environmental applications and consequently the undisputed player of the so-called first generation of photoactive materials[5, 6]. Semiconducting oxides owe their photoactivity to the ability of exciting electrons, under irradiation with light of suitable frequency, from the valence band (VB) to the conduction band (CB) thereby creating holes in the valence band itself[7]. Due to their reductive (electrons) and oxidative (holes) potentials the photoexcited charge carriers, once they reach the surface, are able to entail redox chemical reactions. The limitation of this approach relies in the irreconcilable divergence between the width of the oxide band gap and the redox potential of the excited charge carriers. By increasing the band gap of the oxide, the electrochemical potentials of excited electrons and holes become more effective, but, at the same time, photoexcitation implies to use photons of higher energy. Pristine TiO_2 is efficient in decomposing pollutants under irradiation with ultraviolet light (band gap around 3.2eV) but is poorly effective under sunlight as this contains prevalently visible and near-infrared (NIR) radiation.

Photoactive solid systems capable to use visible light for the charge separation have been the target of a continuous search during the past twenty years. The research has mainly focused on the modifications of TiO_2 via doping with transition metal ions[8], p-block elements[9-11], or supported metal nanoparticles[12] having plasmonic effects. All these systems constitute the body of the so called second generation photoactive materials[5] based on titanium dioxide. In general, however, to this generation belong also other and even more complex materials[dci1].

The possible role in photocatalytic phenomena of other oxides having appropriate flat-band potentials, has been partly neglected in the past. Zirconium dioxide, for instance, a ceramic material also used as heterogeneous catalysts, has found only few applications in photocatalysis[13] because of its large band gap (*ca.* 5.0 eV), an energy corresponding to a negligible fraction of the solar light at earth surface.

In the present paper we show that materials based on ZrO_2 modified by dispersion of Ce^{4+} ions in the bulk become photosensitive to visible light. This effect is due to the interplay between the energy levels of the two components. The photoactivity of the solids has been investigated mainly via Electron Paramagnetic Resonance (EPR) monitoring the formation of both charge carriers (electrons and holes) and OH radicals under irradiation with visible frequencies. DFT calculations provide a rational of the change in electronic structure and optical properties upon Ce doping. The Ce-ZrO_2 system here described is probably the first example of third generation photocatalytic materials based on a double excitation through localized intra-bandgap states, a mechanism recently proposed by Serpone et al. and still waiting for experimental confirmation[5, 6].

The CeO_2 molar fraction of the mixed oxide employed for the present investigation is 0.5% (CZ05). This material will be hereafter labeled as CZ05. Samples of the two bare oxides were also prepared and used to compare their properties with those of the mixed oxide.

For the mixed sample two phases have been identified by XRD analysis (S.I.): tetragonal (t) and monoclinic (m) zirconia (Table 1). The fraction of monoclinic phase is higher for Ce-doped ZrO_2 than that found for the pure phase probably because a partial disorder in the structure is induced by Ce addition.

Table 1. Weight percentage (%wt) and crystallite size (d) obtained from Rietveld refinement of the XRD patterns of bare and mixed Ce-Zr oxides. SBET is the surface area derived from nitrogen adsorption measurements

Sample	Phase	%wt	d (nm)	S_{BET} (m^2/g)
ZrO_2	t-ZrO_2	78	15	150
	m-ZrO_2	22	15	
CZ05	t-ZrO_2	57	16	66
	m-ZrO_2	43	12	
CeO_2	c-CeO_2	100	12	55

The optical properties of CZ05 were measured by Diffuse Reflectance UV-Vis spectroscopy. Figure 1 compares the behavior of the mixed material with that of both pure oxides. The extreme features of this series are represented by the band gap transitions of zirconia and ceria which fall at 244 and 477 nm (5.08 eV and 2.60 eV), respectively. The latter is due to the excitation of electrons from the VB to Ce 4f orbital states[14]. The CZ05 UV-Vis absorption, even with such a low amount of ceria, shows a red shift in comparison to the band gap transition of ZrO_2 with a weak tail in the visible. Remarkably, a solid produced by prolonged mechanical mixing of ZrO_2 and CeO_2 and having the same composition of CZ05 has an optical behavior practically coincident with that of bare ZrO_2 (magnification in Fig. 1B). This firmly indicates that the preparation procedure adopted favors an intimate interaction of Ce^{4+} and ZrO_2 conferring peculiar optical properties to the mixed solid.

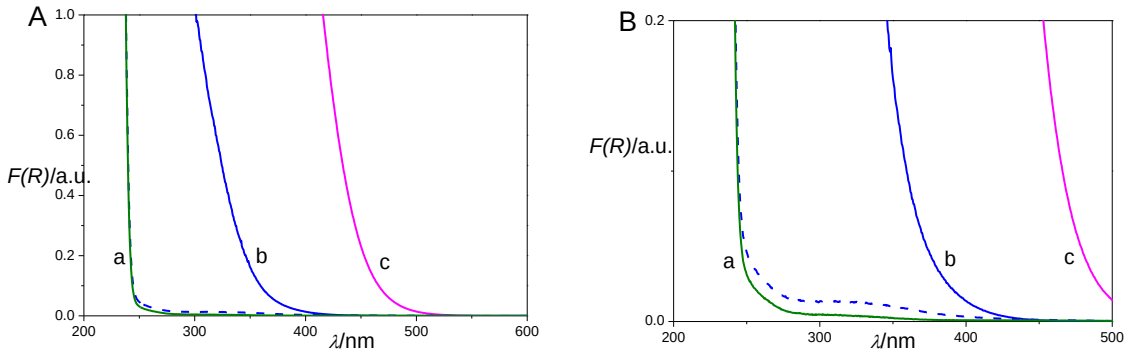

Figure 1. A) Absorption spectra of a) ZrO_2, b) CZ05, c) CeO_2. B) magnification of A. The dashed line is related to a mechanical mixture with the same composition of CZ05.

The photoactivity of the mixed material has been tested by EPR. This is a suitable technique to detect the charge separation, as shown by the seminal work of Graetzel and Howe[15] and by that of the Thurnauer group[16] who monitored by EPR the formation of both photoexcited electrons and holes in UV irradiated TiO_2.

We have followed (Fig. 2A) the charge separation in the case of Ce-ZrO_2 using irradiation with visible light, that is applying a cut off to the lamp output at 420nm. The starting spectrum (Fig. 2A, a) does not show a flat baseline and the EPR signal observed (nearly axial with $g_{\|}$=1.977 and $g_{\perp}$=1.959) is the same observed in the case of bare ZrO_2 and due to Zr^{3+} ions always present as defects in this solid[17]. Irradiation of the CZ05 sample at 77K with light having λ>420nm (i.e. $h\nu$<2.95eV) (Fig. 2A, b) causes the intensity increase of the Zr^{3+} signal and, in parallel, the appearance of a new signal due to trapped holes (O^- ions) at lower field[17]. Heating the system at RT, electrons and holes quickly recombine, recovering the initial situation.

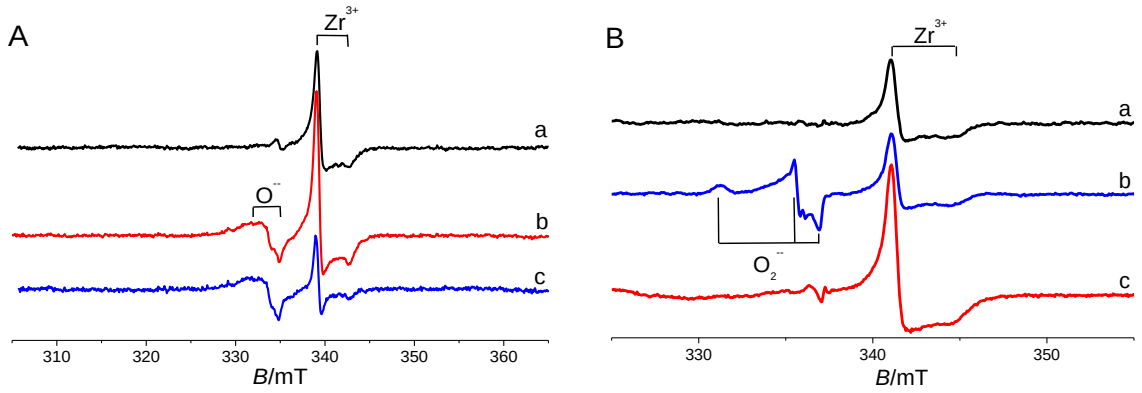

Figure 2. EPR spectra of CZ05 recorded at 77K under irradiation with visible light (λ>420nm). A: irradiation under vacuum (a, background; b, irradiation; c, difference spectrum(b-a)). B: irradiation in gas atmosphere (a, background; b, O2; c, H2).

The effective charge separation occurring under irradiation is better evidenced by subtracting the background from the spectrum obtained upon irradiation. The spectrum (Fig. 2A, c) shows two equally intense and distinct signals (O^-, Zr^{3+}) which derive from the charge separation. It is worth mentioning that this effect has been obtained using wavelengths belonging entirely to the visible light domain. The same experiment, performed on bare ZrO_2, has no appreciable effects. The spectra in Fig. 2A are conceptually important as they clearly indicate that: a) the insertion of small amounts of cerium sensitizes the ZrO_2 matrix to visible light and b) the visible-light excited electrons reach the conduction band of ZrO_2 forming Zr^{3+} ions. This result is strengthened by parallel experiments (Fig. 2B) consisting in the irradiation of the material under an atmosphere of either O_2 or H_2 which allows to demonstrate that the generated charge carriers actually reach the surface of the nanoparticles. In the former case, in fact, O_2 reacts with photo-generated electrons producing surface adsorbed superoxide, O_2^-:

$$e^-_{(CB)} + O_{2\,(gas)} \rightarrow O_2^-{}_{(ads)} \qquad (1)$$

Fig 2B, b shows the well known spectrum of O_2^- adsorbed on the ZrO_2 surface[17] which proves that electrons photoexcited in conduction band have reached the surface.

In the second case, holes (h^+) react with gas-phase hydrogen at the surface yielding surface OH^- groups and injecting electrons in the solid[18] which are stabilized by zirconium ions forming reduced Zr^{3+} centres:

$$h^+ + O^{2-}_{(surf)} \rightarrow O^-_{(surf)} \quad (2)$$

$$O^-_{(surf)} + H_2 \rightarrow OH^-_{(surf)} + H^\bullet \quad (3)$$

$$H^\bullet + O^{2-}_{(surf)} + Zr^{4+} \rightarrow OH^-_{(surf)} + Zr^{3+} \quad (4)$$

Fig. 2B, c reports the intensity increase of the Zr^{3+} signal (eq. 4) produced by visible light irradiation in H_2 and attesting the presence of holes at the surface .

The two parallel experiments illustrated in Fig. 2B confirm that visible photons induce electron-hole separation in Ce-doped zirconia (Fig. 2A) adding the important information that both carriers reach the surface and are, in principle, available for surface reactions.

The potential photocatalytic activity of the Ce-ZrO_2 system in visible light was tested monitoring the formation of hydroxyl radicals ($HO^\bullet$) upon irradiation of a water suspension of the CZ05 sample. $HO^\bullet$ radicals, which are responsible of the oxidative attack of organic molecules in photocatalytic reactions, are formed according to:

$$h^+ + H_2O \rightarrow HO^\bullet + H^+ \quad (5)$$

Due to their reactivity, these radicals can only be detected in solution by means of a spin trap (namely the 5,5-dimethyl-1-pyrroline N-oxide, DMPO), a diamagnetic molecule which, by reaction with $HO^\bullet$, forms a relatively stable radical adduct detected by EPR. The detection of photoinduced $HO^\bullet$ radicals is thus an evidence of the oxidative ability of an irradiated solid[19]. Figure 3A reports the EPR spectra obtained upon illumination of a CZ05 aqueous suspension

with visible light at various times. All spectra are amenable to the typical four lines signal of the DMPO/HO• adduct and have been obtained subtracting from the experimental spectrum that of a reference obtained irradiating a solution of DMPO. The reported spectra are thus entirely due to the effect of the solid material. Figure 3B shows that the intensity of the adduct becomes appreciable after 10 min irradiation and reaches a maximum after about 110 min. Also in this case no effect is observed using pure ZrO_2.

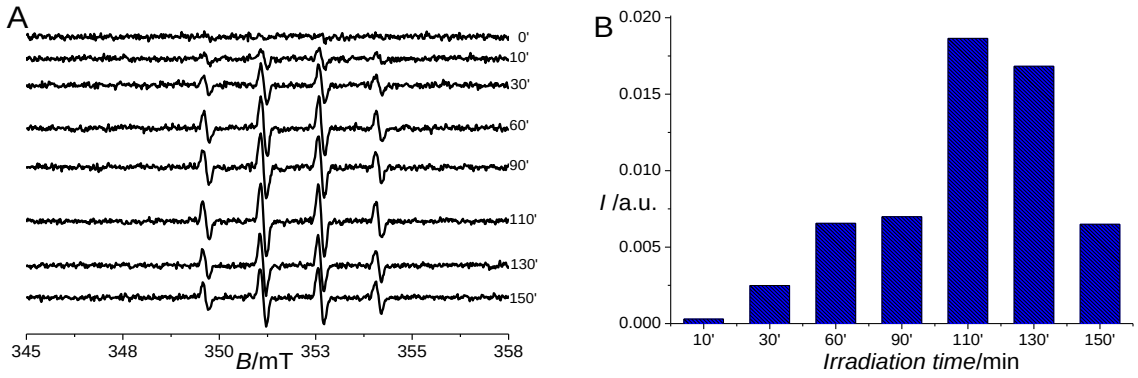

Figure 3. A. EPR spectra of the DMPO/HO• adduct produced by irradiation of an aqueous suspension of CZ05 with Visible-NIR light (λ>420nm) as a function of the irradiation time. B. Bar diagram of the corresponding EPR intensities.

The origin of the visible light photoactivity of Ce-doped ZrO_2 can be understood based on DFT (B3LYP) calculations. Hybrid exchange-correlation functionals, making use of a combination of exact (as in HF) and DFT exchange terms, were shown in recent years to quite accurately reproduce experimental band gaps, which on the contrary are severely underestimated by local or semilocal functionals[20]. Zr and Ce atoms are isovalent. Therefore, the replacement of a Zr ion with a Ce ion in the same formal +4 oxidation state does not alter the charge neutrality of the system and does not result in extra electrons in the electronic structure. The incorporation of Ce in substitutional positions of the ZrO_2 tetragonal lattice creates a series of unoccupied

defect states in the band-gap (direct: 5.8 eV, 5.6 for the monoclinic phase), about 3.2-3.5 eV above the top of the VB, Figure 4 (Kohn-Sham energy levels). Projection of these bands onto the basis functions of the Ce atom indicates that they originate from the Ce 4f states and that are highly localized around Ce. Virtually no dispersion is observed for the case of an isolated Ce ion.

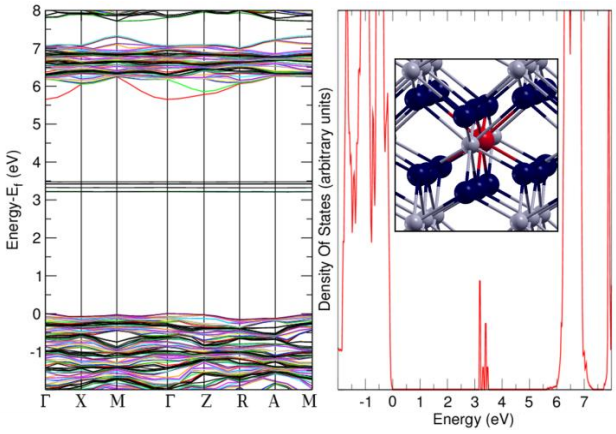

Figure 4. Band structure (left) and density of states (right) of a 3x3x2 tetragonal ZrO_2 supercell doped with a single substitutional Ce atom (inset).

Very important for the interpretation of the results is the calculation of the energies involved in electronic transitions stimulated by irradiation with visible light. It is common practice to estimate the semiconductor band gap and the energy levels introduced in the gap by defect centers using the single-particle Kohn-Sham eigenvalues. This approach, however, is not well justified if electronic transitions are involved. A more robust approach consists in the calculation of transition energy levels between different charge states for a defective system. The transition level $\varepsilon(q+1/q)$ is defined as the Fermi-level, referred to the top of the valence band, for which the formation energies of defect in the charge states $q+1$ and q are equal. In general, the transition energy levels can be derived from calculated total energies. With the CRYSTAL code used for the calculations, they are approximated, on the basis of Janak's theorem, from single particles eigenvalues[21]. This method is rather accurate when used in connection with hybrid functionals

that provide a good estimate of the Kohn-Sham band gap of the system[22]. In particular, optical transition levels (ε^{opt}) can be directly compared with the position of the defect levels estimated from optical excitation, Figure 5. Two transitions are of particular importance here:

$$O^{2-}_{(VB)} + Ce^{4+} \rightarrow O^{-}_{(VB)} + Ce^{3+} \quad (6)$$

$$Ce^{3+} + Zr^{4+}_{(CB)} \rightarrow Ce^{4+} + Zr^{3+}_{(CB)} \quad (7)$$

The results show that the transition from the VB to a Ce^{4+} cation, eq. 6, leading to a Ce^{3+} ion, occurs at 2.5 eV, i.e. well inside the visible light spectrum. A second excitation can occur from these states with an electron transfer from Ce^{3+} to the CB, eq. 7: in this case, the optical transition is found at 3.3 eV (3.1 + 0.2 eV, Fig 5) i.e. at the limit of the visible light radiation (the 0.2 eV contribution is due to the formation of localized Zr^{3+} states just below the CB minimum, as discussed in ref. 17). This second excitation value is probably too large since the B3LYP method overestimates the conduction band minimum (CBM) energy and thus the band gap of ZrO_2 by 14% (KS gap 5.8 eV, Fig. 5, experimental optical transition 5.1 eV, Fig. 1). Therefore, we propose these transitions from the VBM (valence band maximum) to the Ce^{4+} states and from the Ce^{3+} states to the CBM to be at the origin of the optical absorption spectrum in Fig. 1b (where the absorption edge of the doped sample falls below the 3 eV threshold) and consequently of the formation of O^- and Zr^{3+} species observed experimentally under visible light irradiation

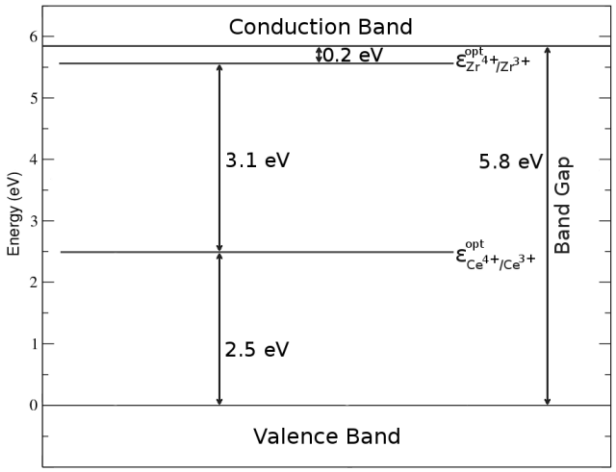

Figure 5. Optical transition levels for a 3x3x2 tetragonal ZrO_2 supercell doped with a single Ce atom dopant. The position of both mid gap Ce^{3+} states and defective Zr^{3+} ones is indicated.

To conclude, the set of data discussed above indicates that it is possible, through the dispersion of small amounts of cerium ions, to make ZrO_2 photosensitive to visible light. Based on the available experimental and theoretical data, a possible explanation points to the role of intraband gap Ce 4f empty states which could act as a bridge between the valence band and the conduction band of the oxide allowing low-energy photons to excite electrons from one band to the other. The mechanism corresponds to one of the two proposed by Serpone et al. while forecasting the nature of third generation photocatalysts[5, 6]. Ce-ZrO_2 can therefore be considered as the first member of this new family. Despite the system described shows an effective photoactivity, the results presented represent a "proof of concept" and show that this new class of photo-active materials can indeed be prepared. Further work is necessary to identify the optimal working conditions (Ce loading, crystal structure and morphology, preparation procedures etc.) and to optimize the activity and selectivity performances of the present system not only under visible light but also under real solar light irradiation.

EXPERIMENTAL METHODS

Mixed Ce-Zr oxides were prepared via sol-gel synthesis using Ce isopropoxide and Zr propoxide solutions and following a complex procedure fully described in the S.I. The sol produced by hydrolysis was aged in air until the formation of a gel which was then dried at 333K. Finally the powder was calcined at 723 K in air for 2 hours.

Details on the experimental characterization methods, namely Powder X-rays diffraction (XRD), surface area measurements, Diffuse Reflectance UV-Vis (DR-UV-Vis) spectroscopy, EPR spectroscopy and Spin Trapping are available as S.I.

Spin-polarized periodic DFT (B3LYP) calculations were performed using the CRYSTAL09 code, based on a linear combination of atomic orbitals (LCAO). Further details on the models, the basis sets and the computation of the transition energy levels are illustrated in S. I.

ASSOCIATED CONTENT

Supporting Information. Additional information are available on (1) synthesis procedure; (2) experimental methods; (3) computational details; (4) X-ray diffraction patterns; (5) additional calculations on the effect of Ce concentration. This material is available free of charge via the Internet at http://pubs.acs.org.

AUTHOR INFORMATION

Corresponding Author

*Email: elio.giamello@unito.it

Notes

The authors declare no competing financial interests.

ACKNOWLEDGMENT

This work has been supported by the Italian Ministry of University and Research, MIUR, through the "Programs of National Relevance" (PRIN-2009); the "National Funding for Basic Research" (FIRB) with a project entitled "Oxides at the nanoscale: functionalities and applications" (FIRB RBAP11AYN).

REFERENCES

(1) Fujishima, A.; Zhang, X.; Tryk, D. A. TiO_2 Photocatalysis and Related Surface Phenomena. *Surf. Sci. Rep.* **2008,** *63*, 515-582.
(2) Hagfeldt, A.; Gratzel, M. Light-Induced Redox Reactions in Nanocrystalline Systems. *Chem. Rev.* **1995,** *95*, 49-68.
(3) Fujishima, A.; Honda, K. Electrochemical Photolysis of Water at a Semiconductor Electrode. *Nature* **1972,** *238*, 37-38.
(4) Gust, D.; Moore, T. A.; Moore, A. L. Solar Fuels via Artificial Photosynthesis. *Acc. Chem. Res.* **2009,** *42*, 1890-1898.
(5) Emeline, A. V.; Kuznetsov, V. N.; Ryabchuk, V. K.; Serpone, N. On the Way to the Creation of Next Generation Photoactive Materials. *Environ. Sci. Pollut. Res.* **2012,** *19*, 3666-3675.
(6) Serpone, N.; Emeline, A. V. Semiconductor Photocatalysis - Past, Present, and Future Outlook. *J. Phys. Chem. Lett.* **2012,** *3*, 673-677.
(7) Linsebigler, A. L.; Lu, G. Q.; Yates, J. T. Photocatalysis on TiO_2 Surfaces - Principles, Mechanisms, and Selected Results. *Chem. Rev.* **1995,** *95*, 735-758.
(8) Takeuchi, M.; Yamashita, H.; Matsuoka, M.; Anpo, M.; Hirao, T.; Itoh, N.; Iwamoto, N. Photocatalytic Decomposition of NO Under Visible Light Irradiation on the Cr-Ion-Implanted TiO_2 Thin Film Photocatalyst. *Catal. Lett.* **2000,** *67*, 135-137.
(9) Asahi, R.; Morikawa, T.; Ohwaki, T.; Aoki, K.; Taga, Y. Visible-Light Photocatalysis in Nitrogen-Doped Titanium Oxides. *Science* **2001,** *293*, 269-271.
(10) Livraghi, S.; Paganini, M. C.; Giamello, E.; Selloni, A.; Di Valentin, C.; Pacchioni, G. Origin of Photoactivity of Nitrogen-Doped Titanium Dioxide Under Visible Light. *J. Am. Chem. Soc.* **2006,** *128*, 15666-15671.
(11) Barolo, G.; Livraghi, S.; Chiesa, M.; Paganini, M. C.; Giamello, E. Mechanism of the Photoactivity under Visible Light of N-Doped Titanium Dioxide. Charge Carriers Migration in Irradiated N-TiO_2 Investigated by Electron Paramagnetic Resonance. *J. Phys. Chem. C* **2012,** *116*, 20887-20894.
(12) Warren, S. C.; Thimsen, E. Plasmonic Solar Water Splitting. *Energy Environ. Sci.* **2012,** *5*, 5133-5146.
(13) Kohno, Y.; Tanaka, T.; Funabiki, T.; Yoshida, S. Identification and Reactivity of a Surface Intermediate in the Photoreduction of CO_2 with H_2 over ZrO_2. *J. Chem. Soc. Faraday Trans.* **1998,** *94*, 1875-1880.
(14) Da Silva, J. L. F.; Ganduglia-Pirovano, M. V.; Sauer, J.; Bayer, V.; Kresse, G. Hybrid Functionals Applied to Rare-Earth Oxides: the Example of Ceria. *Phys. Rev. B* **2007,** *75*, 035109.
(15) Howe, R. F.; Gratzel, M. Electron-Paramagnetic-Resonance Study of Hydrated Anatase Under UV Irradiation. *J. Phys. Chem.* **1987,** *91*, 3906-3909.

(16) Micic, O. I.; Zhang, Y. N.; Cromack, K. R.; Trifunac, A. D.; Thurnauer, M. C. Photoinduced Hole Transfer from TiO_2 to Methanol Molecules in Aqueous-Solution Studied by Electron-Paramagnetic-Resonance. *J. Phys. Chem.* **1993,** *97*, 13284-13288.
(17) Gionco, C.; Paganini, M. C.; Giamello, E.; Burgess, R.; Di Valentin, C.; Pacchioni, G. Paramagnetic Defects in Polycrystalline Zirconia: An EPR and DFT Study. *Chem. Mater.* **2013,** *25*, 2243-2253.
(18) Livraghi, S.; Chiesa, M.; Paganini, M. C.; Giamello, E. On the Nature of Reduced States in Titanium Dioxide As Monitored by Electron Paramagnetic Resonance. I: The Anatase Case. *J. Phys. Chem. C* **2011,** *115*, 25413-25421.
(19) Dvoranova, D.; Brezova, V.; Mazur, M.; Malati, M. A. Investigations of Metal-Doped Titanium Dioxide Photocatalysts. *Appl. Catal. B* **2002,** *37*, 91-105.
(20) Muscat, J.; Wander, A.; Harrison, N. M. On the Prediction of Band Gaps from Hybrid Functional Theory. *Chem. Phys. Lett.* **2001,** *342*, 397-401.
(21) Gallino, F.; Pacchioni, G.; Di Valentin, C. Transition Levels of Defect Centers in ZnO by Hybrid Functionals and Localized Basis Set Approach. *J. Chem. Phys.* **2010,** *133*, 144512.
(22) Oba, F.; Togo, A.; Tanaka, I.; Paier, J.; Kresse, G. Defect Energetics in ZnO: A Hybrid Hartree-Fock Density Functional Study. *Phys. Rev. B* **2008,** *77*, 245202.

Cerium Doped Zirconium Dioxide, a Visible-Light Sensitive Photoactive Material of Third Generation

Chiara Gionco[1], Maria Cristina Paganini[1], Elio Giamello[1*], Robertson Burgess[2], Cristiana Di Valentin[2], Gianfranco Pacchioni[2].

[1] Dipartimento di Chimica, Università di Torino and NIS, Nanostructured Interfaces and Surfaces, Via P. Giuria 7, 10125 Torino, Italy

[2]Dipartimento di Scienza dei Materiali, Università di Milano-Bicocca, Via R. Cozzi, 53, 20125, Milano, Italy

Supporting Information

Preparation of the samples

To prepare CZ05, 0.024g of $Ce(OC_3H_7)_4$ were dissolved in 5ml of C_3H_7OH. Then 5.4ml of $Zr(OC_3H_7)_4$ were added to the solution and finally 3ml of double distilled water were added to start hydrolysis. The sol produced by hydrolysis was aged in air until the formation of a gel which was then dried at 333K. Finally the powder was calcined at 723 K in air for 2 hours.
Pure ZrO_2 and CeO_2 were prepared starting from the same precursors in analogous way.

Characterization techniques

Powder X-rays diffraction (XRD) patterns were recorded with a PANalytical PW3040/60 X'Pert PRO MPD using a copper K_α radiation source (0.15418 nm). The intensities were obtained in the 2θ ranges between 20° and 80°. The X'Pert High-Score software was used for data handling. The MAUD 2.26 [1] software was used for Rietveld refinement. To determine the instrumental function the pattern obtained by a well crystallized silicon standard (crystallite size = 1 μm) was used.
The surface area measurements were carried out on a Micromeritics ASAP 2020/2010 using the Brunauer-Emmett-Teller (BET) model on the N_2 adsorption measurement. Prior to the adsorption run, all the samples were outgassed at 573K for 3 h.
The UV-Vis absorption spectra were recorded using a Varian Cary 5 spectrometer, coupled with an integration sphere for diffuse reflectance studies, using a Carywin-UV/scan software. A sample of PTFE with 100% reflectance was used as reference.
Electron Paramagnetic Resonance (EPR) spectra, recorded at room temperature and at liquid nitrogen temperature, were run on a X-band CW-EPR Bruker EMX spectrometer equipped with a cylindrical cavity operating at 100 kHz field modulation. The effect of light on EPR spectra was investigated irradiating the sample in the EPR resonant cavity by a 1000 W mercury/Xenon lamp (Oriel Instruments) equipped with a IR water filter to avoid over-heating.
The generation of radical species in solution was monitored by the EPR-spin trapping technique using a Miniscope 100 spectometer from Magnettech and DMPO (5,5-dimethyl-1-pyrroline-N-oxide, Alexis Biochemicals, San Diego, CA) as spin trapping agent.

Computational details

Spin-polarized DFT calculations were performed using the CRYSTAL code based on a linear combination of atomic orbitals (LCAO). The hybrid B3LYP functional which gives a good estimate of the Kohn-Sham band gap has been used in all calculations. A 8-4111(d1) Gaussian-type basis set was used for the O atoms; for Zr we used a 311(d31) basis set associated with the Hay and Wadt effective core pseudopotential (ECP); for Ce we used 4321(d61)(f431) basis set associated with the Stuttgart-Dresden effective core potential. The reciprocal space is sampled using a regular sublattice with a shrinking factor of 2, and the SCF convergence was set to 10^{-6} a.u.

A 108-atoms 3x3x2 supercell was generated for the calculations. Full geometry relaxation (atom locations and cell parameters) was performed with no symmetry constraint using a Broyden-Fletcher-Goldfarb-Shanno scheme. The convergence criteria was set to an RMS of the gradient of $3x10^{-4}$ a.u. and an RMS of the maximum atomic displacement of $1.2x10^{-3}$ a.u. The computed cell parameters of pure tetragonal ZrO_2, P42/nmc space group, a = 3.6055 Å and c = 5.1797 Å, are in reasonable agreement with previous calculations and experimental results[2]. Each Zr atom has 4 nearest neighbour O atoms at a distance of 2.06 Å and another 4 next-nearest neighbour O atoms at a distance of 2.40 Å. The band-gap of ZrO_2 computed at the B3LYP level at the Γ point is about 5.8 eV. This is significantly higher than the measured bandgap of 4.2 eV using electron energy loss spectroscopy (EELS)[3] but within the range measured using vacuum-ultraviolet (VUV) absorption spectroscopy (5.78-6.62 eV)[2]. The VB is dominated by the O 2p states, and the CB is dominated by the Zr 4d states.

Different concentrations and arrangements of Ce atoms substituting Zr atoms in the zirconia lattice were considered. The lowest concentration, corresponding to 1 Ce every 36 Zr ions, is 2.8%. Doping levels of 2 and 5 Ce atoms per supercell (5.5 and 13.9%, respectively) were also considered, in configurations where the Ce atoms are either clustered together or spread throughout the supercell. Systems with an extra electron added were treated by adding a uniform background charge to the supercell.

Transition energy levels were calculated using a method outlined in previous publications. The vertical or optical transition energy from a state of charge q+1 to a state of charge q of a general defect D can be calculated as:

$$\varepsilon(q+1/q) = E_{D,q} - E_{D,q+1} = [e_{LUMO}(N-1) + e_{HOMO}(N)]/2 \quad (1)$$

where $e_{HOMO}(N)$ is the energy of the highest occupied crystal state of the system of in charge state q, and $e_{LUMO}(N-1)$ is the energy of the lowest unoccupied crystal state of the system of charge q+1, with both energies referenced to the top of the VB which is set as the zero energy level.

X-Ray powder diffraction analysis

Figure S1 shows the XRD patterns obtained for pure ZrO_2, pure CeO_2 and CZ05. While in Table S1 all parameters used in the Rietveld refinement done using the MAUD software are reported. From the XRD patterns shown there is no evidence of any reflection peak peculiar of the CeO_2 fluoritic phase.

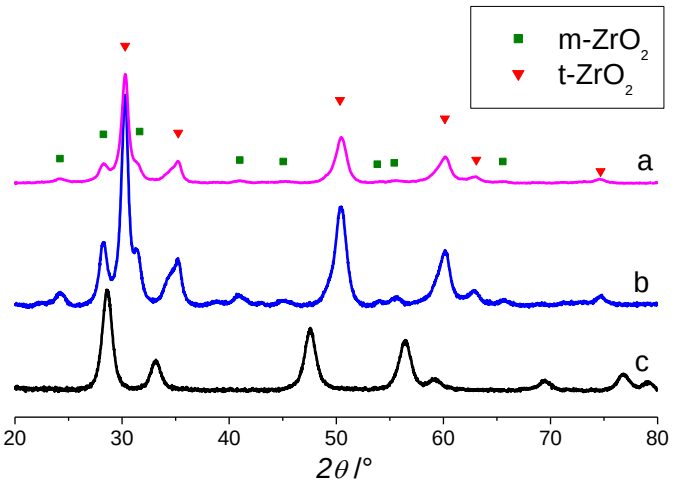

Figure S1. XRD patterns of ZrO_2 (a), CZ05 (b) and CeO_2(c).

Table S1. Weight percentage (%wt) and lattice parameters (a, b, c, β) obtained from Rietveld refinement of the XRD patterns of bare and mixed Ce-Zr oxides. R_{wp} is the weighted residual error.

Sample	R_w	Phase	%wt	a	b	c	β
ZrO_2	4.56	t-ZrO_2	78	3.60	3.60	5.17	/
		m-ZrO_2	22	5.15	5.21	5.32	98.72
CZ05	1.45	t-ZrO_2	57	3.60	3.60	5.18	/
		m-ZrO_2	43	5.15	5.20	5.33	99.00
CeO_2	2.74	c-CeO_2	100	5.41	5.41	5.41	/

DRS characterization of mechanical mixtures

Figure S2 reports a diffuse reflectance spectroscopy comparison between two mechanical mixtures having different CeO_2 molar concentration. Increasing the CeO_2 content from 0.5% to 10% a band with position matching that of pure CeO_2 appears. It is noteworthy that the absorption at lower frequencies that the energy band gap of pure zirconia of the mechanical mixture with 10% of CeO2 is less than that of our sample doped with 0.5% Ce concentration (see Fig.1). This phenomenon indicates again that doping deeply modifies the electronic structure of the material.

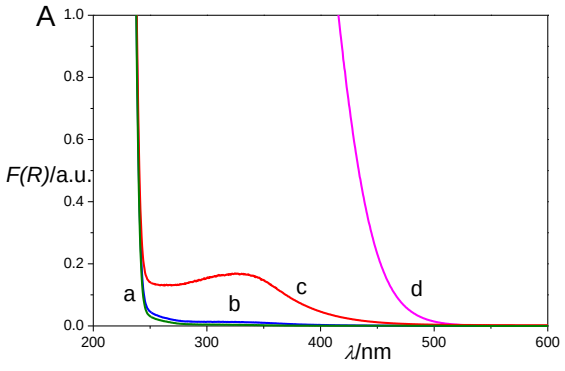

Figure S2. Absorption spectra of a) ZrO_2, b) CZ05 mechanical mixture, c) CZ10 mechanical mixture d) CeO_2.

EPR spectra under visible irradiation for pure ZrO_2

Figure S3 shows the results obtained for pure ZrO_2 while performing the same experiment reported on figure 2A. The slight difference that can be seen by subtracting the starting spectrum from the irradiated spectrum (Fig. S3, trace c) is actually the result of the change in linewidth of the signal under irradiation. Indeed if the integrated area is considered (which is roughly proportional to the number of spins present in the sample) no significant change is can be noticed.

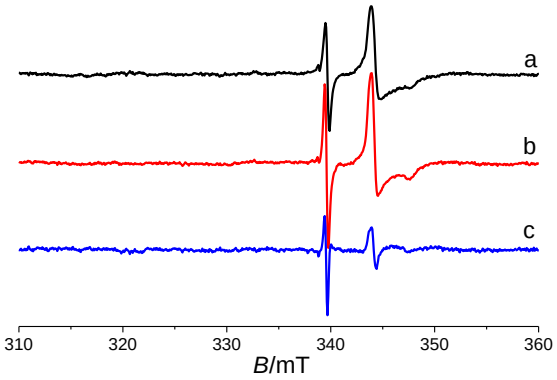

Figure S3. EPR spectra of ZrO_2 recorded at 77K under irradiation with visible light (λ>420nm) under vacuum (a, background; b, irradiation; c, difference spectrum(b-a)).

DFT calculations: effect of Ce concentration

Substitution of more than one Zr atoms for Ce atoms was shown to cause a small broadening of the defect states, Figure S2. Clustering the Ce atoms together resulted in slightly higher dispersion of the defect states. The maximum broadening of the gap state is obtained for the case of five doping Ce atoms grouped together in the 108-atoms supercell (doping level of 13.9%, Figure S4). The total energies of the systems did not vary significantly when Ce atoms were clustered or spread out, and no special indication that the Ce dopants tend to aggregate emerges from the calculations.

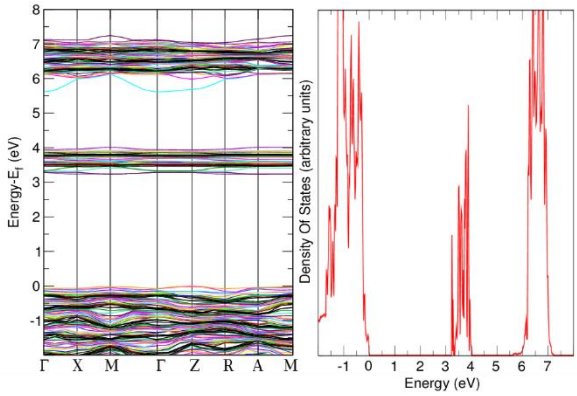

Figure S4. Band structure (left) and density of states (right) of a 3x3x2 tetragonal ZrO_2 supercell doped with 5 substitutional Ce atoms grouped together.

[1] L. Lutterotti, *Nucl. Instrum. Methods Phys. Res. Sect. B* **2010**, 268, 334.
[2] R. H. French, S. J. Glass, F. S. Ohuchi, Y. N. Xu, W. Y. Ching, *Phys. Rev. B* **1994**, 49, 5133.
[3] D. W. McComb, *Phys. Rev. B* **1996**, 54, 7094.